

Synthesis of novel (2E)-1-[4-(2,4-difluorophenyl)phenyl]3-arylprop-2-en-1-ones: Investigation on spectral, antibacterial, molecular docking and theoretical studies

M. Fathimunnisa ^a, H. Manikandan ^{a,*}, S. Selvanayagam ^b

^a Department of Chemistry, Annamalai University, Annamalaiagar, 608 002, Tamilnadu, India

^b Department of Physics, Kings College of Engineering, Punalkulam, 613 303, Tamilnadu, India

ARTICLE INFO

Article history:

Received 20 April 2015

Received in revised form

29 May 2015

Accepted 24 June 2015

Available online 2 July 2015

Keywords:

Difluorobiphenyl chalcones

XRD analysis

Solvatochromism

Antimicrobial activity

Molecular docking

1. Introduction

Recently the resistance of bacteria towards the existing anti-bacterial drugs is a major threat across the world. Therefore, the synthesis of biologically active scaffold have been of great interest in the drug discovery [1]. Several popular pharmaceutical drugs like fluorocytosine, fludarabine, panomifene and diflunisal contain fluorine as a part of it because of the increased binding affinity to the target protein. The incorporation of fluorine atom(s) tends to increase the lipophilic nature of the scaffold which is a desirable criteria for the drug design and development [2].

Chalcones (1,3-diaryl-2-propen-1-ones) are interesting class of compounds that occur naturally and exhibit extensive attention for the several years due to their simple structure and diverse pharmacological activities. They act as precursors and valuable intermediates for the synthesis of many biologically important heterocyclic compounds like pyrimidine, isoxazoles, pyrazolines, benzofuranones, flavanones, quinolinones, etc. The presence of three carbon unsaturated carbonyl system between two aromatic

rings show broad range of biological activities including anti-inflammatory [3], anti-malarial [4], anti-bacterial [5], anti-cancer [6–8], anti-tumor [9], anti-HIV [10] and anti-invasive [11].

Some of the naturally occurring chalcones like butein (1) [12], cardamonin (2) [13], isoliquiritigenin (3) [14], licochalcone A (4) and Xanthohumol (5) [15] exhibit anticancer and antimicrobial activities (Fig. 1). The biphenyl moiety is also found in many natural products that exhibits a wide variety of biological activities such as anti-cancer [16–19], anti-angiogenic [16,18], anti-viral [20] and have the ability to display enhanced fluorescence [21]. The emerging application of chalcones, fluorine and biphenyl initiate us to synthesize some novel difluorobiphenyl chalcones.

Previously, the monofluorobiphenyl chalcones were reported by Yinglinzuo et al. [22], which exhibit NF-κB inhibition and cancer cell growth inhibition against a panel of cancer cell lines (A549, CNE2, SW480, MCF-7, HepG2). Although many heterocyclic chalcones and biaryl chalcones were reported, the difluorobiphenyl chalcones have been studied rarely.

The present study report the synthesis, characterization and antimicrobial evaluation against bacterial (gram-positive and gram-negative) strains by disc diffusion and serial dilution method. The compound (2E)-1-(2',4'-difluorobiphenyl)-3-phenylprop-2-en-1-one (7) was chosen as a representative to gain insight on the molecular geometry (experimental and theoretical) of the synthesized compounds. In addition to explore the scope of our study the molecular docking studies against cancer protein 4LRH were performed.

2. Experimental

2.1. General

All the chemicals and solvents were of analytical grade and used without further purification. Melting points of the synthesized compounds have been measured in open glass capillaries and were uncorrected. The FT-IR spectra were recorded on AVATAR-330 FT-IR spectrophotometer. The sample was mixed with KBr and pellet technique was adopted to record the spectra in cm^{-1} . The NMR

* Corresponding author. Department of Chemistry, Annamalai University, Annamalaiagar, 608 002, Tamilnadu, India.

E-mail address: profmani.au@gmail.com (H. Manikandan).

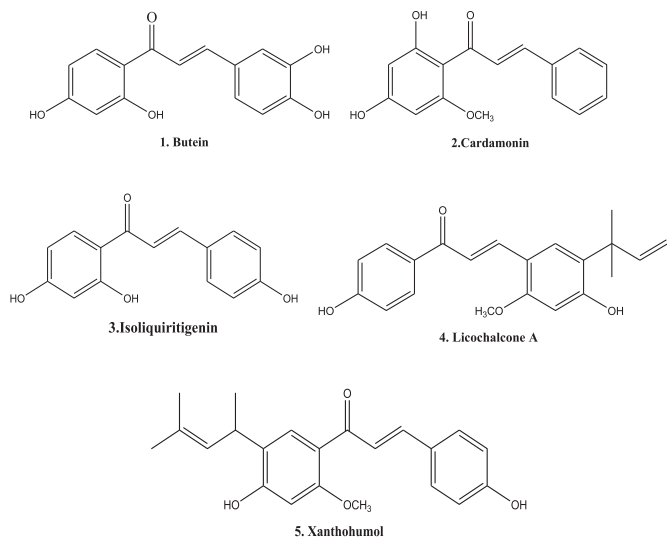


Fig. 1. Structure of some naturally occurring chalcones.

spectra of all the compounds were recorded on a BRUKER Avance III 400 MHz spectrometer operating at 400 MHz for ^1H , 125 MHz for ^{19}F and 100 MHz for ^{13}C spectra. The two-dimensional spectra in NMR were performed using standard pulse sequences. The chemical shifts are reported in (δ) units ppm relative to the internal standard Tetra methyl silane (TMS) for ^1H , ^{13}C and C_6F_6 for ^{19}F spectra. The splitting patterns like singlet, doublet, triplet, quartet and multiplet in ^1H NMR are represented as (s), (d), (t), (q) and (m) respectively. The coupling constants (J) were expressed in Hz. Mass spectra have been recorded on SCIEX-API 2000 spectrometer. UV-vis spectra were carried out in SHIMADZU UV-1650 PC digital spectrophotometer by dissolving the sample in special grade ethanol using 1 cm path length quartz cell. The fluorescence spectra were recorded at room temperature on Perkin Elmer LS 55 fluorescence spectrometer and the excitation wavelength (300 nm) was selected based on the absorbance spectrum.

2.2. X-ray analysis

2.2.1. Intensity data collection

Accurate unit cell parameters and orientation matrix were obtained by least-squares fit of several high angle reflections in the range $2.49^\circ \leq \theta \leq 25.89^\circ$ using Mo $K\alpha$ radiation on Bruker SMART APEX CCD area detector using φ and ω scan modes. Cell refinement and data reduction were carried out using SAINT program. A total of 3262 reflections were collected, resulting in 2022 independent reflections had $I > 2\sigma(I)$ and these were considered as observed. The intensities were corrected for Lorentz and polarization effects.

2.2.2. Structure solution and refinement

The structure was solved by direct methods procedure as implemented in SHELXS97 program. The position of all the non-hydrogen atoms were included in the full-matrix least squares refinement using SHELXL2013 program. After few cycles of anisotropic refinement, hydrogen atoms were fixed geometrically and allowed to ride on their parent atoms. The refinement converged to final R-factor of 5.7%. The residual electron density in the final difference Fourier maps has maximum and minimum values of 0.171 and $-0.206 \text{ e}\text{\AA}^{-3}$.

CCDC1060166 contains the supplementary crystallographic data for the title compound. These data can be obtained from free of charge from the Cambridge Crystallographic Data Centre via www.ccdc.cam.ac.uk/data_request/cif.

2.3. Computational details

Computational calculations on compound 7 were carried out by Gaussian 03 W package. The HOMO-LUMO energies were calculated based on the optimized structure in gas phase using TD-DFT/6-31 G (d, p) basis set [23].

2.4. Antimicrobial assay

2.4.1. Collection of bacterial strains

The Clinical isolates of bacterial strains viz., *Staphylococcus aureus*, *Bacillus subtilis*, *Escherichia coli*, *Klebsiella pneumoniae* and *Pseudomonas aeruginosa*. These strains were obtained from the Department of Microbiology, Rajah Muthiah Medical College and Hospital, Annamalai University, Annamalainagar, Tamil Nadu, India. The strains were inoculated on a sterile medium and sub-cultured on to Mueller Hinton Agar plates, these strains are maintained on agar slant at 4°C .

2.4.2. Disc diffusion assay

Antimicrobial activity was performed by the disc diffusion method. About 1 mg/mL stock solution was prepared by dissolving the test compounds (7–14) in 50% DMSO. The sterile paper disc with 6 mm diameter was impregnated with concentration of 200 $\mu\text{g}/\text{mL}$ and the discs were placed in seeded agar plates. The plates were incubated at 37°C for bacteria in incubator. The zone of inhibition for bacteria was visually examined at 37°C for 24 h. Ciprofloxacin was used as a standard positive control for bacteria. Inhibition zones were measured and compared with the standard positive controls. All the tests were carried out in triplicate.

2.4.3. Minimum inhibitory concentration (MIC)

Dilution susceptibility testing method was used for MIC determination with reference to the cited literature [24]. The test compounds were dissolved in 1 ml of chloroform. The different test concentrations of test compounds were 200 – 3.125 $\mu\text{g}/\text{mL}$. It was then serially diluted in to two folds. Where in, 100 μl of sterile Mueller Hinton Broth was decanted into each well of a sterile 96-well micro plate. Highest concentration of the test compounds added at 100 μl to the first well. After mixing of the above, 100 μl of the same was transferred to the second well and in this way, the dilution procedure was continued as a series of dilution of 200 – 3.125 $\mu\text{g}/\text{mL}$ respectively. Inoculum solution at 5 μl was added to every well. Being incubated for 24 h at 37°C , the tubes were monitored for turbidity as growth and non turbidity as no growth. The MIC values were interpreted as the highest dilution (lowest concentration) of the sample, which showed clear fluid with no development of turbidity. Ciprofloxacin was used as a positive control for bacteria. Bacterial growth was indicated by the measure of a white pellet on well bottom.

2.5. Synthesis of 1-(2', 4'-difluorobiphenyl-4-yl)ethanone (6)

The 1-(2',4'-difluorobiphenyl-4-yl)ethanone was synthesized by Friedel–Crafts acylation reaction. Equimolar mixture of 2',4'-difluorobiphenyl (1 mol) and acetyl chloride (1 mol) was refluxed in the presence of aluminum chloride and dichloromethane. The reaction was monitored by TLC and after the completion of reaction the reaction mixture was poured in the crushed ice. The separated solid was filtered, washed with water and recrystallized with ethanol.

2.6. General procedure for the synthesis of (2E)-1-[4-(2,4-difluorophenyl)phenyl]3-arylprop-2-en-1-ones (7–14)

Equimolar mixture of 1-(2',4'-difluorobiphenyl-4-yl)ethanone (1 mmol) and aryl aldehydes (1 mmol) was dissolved in ethanol (20 ml). The sodium hydroxide in water (10%, 2 ml) was added dropwise to the mixture under constant stirring using magnetic stirrer. The reaction mixture was immersed in the crushed ice to maintain the temperature at about 20 °C. The reaction mixture was stirred vigorously for about 1–2 h until the mixture become thick and the stirring is no longer effective. The reaction mixture was neutralized with dil. HCl and kept in the refrigerator overnight. The product was filtered under vacuum, washed with water, dried and recrystallized from ethanol.

2.6.1. (2E)-1-[4-(2,4-difluorophenyl)phenyl]3-phenylprop-2-en-1-one (7)

Yellow solid; Yield 95%; mp. 102–104 °C; IR (KBr, cm^{-1}): 1666 (C=O), 3094–3021 (aromatic C–H), 2924–2855 (aliphatic C–H), 1597 (C=C), 1098, 1141 (C–F); ^1H NMR (400 MHz, CDCl_3 , δ , ppm): 7.57 (d, 1H, H(2), J = 16 Hz), 7.85 (d, 1H, H(3), J = 16 Hz), 8.10 (d, 2H, H(2'') and H(6'')), 6.97 (m, 2H, H(3') and H(5')), 7.43–7.66 (m, 8H, Ar–H); ^{13}C (100 MHz, CDCl_3 , δ , ppm): 189.9 (C=O), 121.9C(2), 145.1C(3), 104.7C(3'), 111.9C(5'), 159.9C(4'), 162.8C(2'), 124.2–139.4 (Ar–C); ^{19}F (376 MHz, CDCl_3 , δ , ppm): –112.86 (d, 1F, J = 7.52 Hz), –109.84 (d, 1F, J = 7.52 Hz); mass (m/z): 321.1 [M+1]⁺; Anal. Calcd (C₂₁H₁₄F₂O): C 78.74H 4.41%. Found: C 78.68H 4.53%.

2.6.2. (2E)-1-[4-(2,4-difluorophenyl)phenyl]3-(4-methylphenyl)prop-2-en-1-one (8)

Yellow solid; Yield 84%; mp. 138–140 °C; IR (KBr, cm^{-1}): 1657 (C=O), 3074–3031 (aromatic C–H), 2914–2851 (aliphatic C–H), 1596 (C=C), 1100, 1140 (C–F); ^1H NMR (400 MHz, CDCl_3 , δ , ppm): 7.54 (d, 1H, H(2), J = 20 Hz), 7.84 (d, 1H, H(3), J = 16 Hz), 8.09 (d, 2H, H(2'') and H(6'')), 6.98 (m, 2H, H(3') and H(5')), 7.43–7.66 (m, 7H, Ar–H), 2.41 (s, 3H, –CH₃); ^{13}C (100 MHz, CDCl_3 , δ , ppm): 190.1 (C=O), 120.9C(2), 145.2C(3), 104.7C(3'), 111.9C(5'), 159.9C(4'), 162.8C(2'), 124.3–141.3 (Ar–C), 21.6 (CH₃); mass (m/z): 335.0 [M+1]⁺; Anal. Calcd (C₂₂H₁₆F₂O): C 79.03H 4.82%. Found: C 77.94H 4.94%.

2.6.3. (2E)-1-[4-(2,4-difluorophenyl)phenyl]3-(4-fluorophenyl)prop-2-en-1-one (9)

Pale yellow solid; Yield 89%; mp. 142–144 °C; IR (KBr, cm^{-1}): 1664 (C=O), 3084–3041 (aromatic C–H), 2954–2853 (aliphatic C–H), 1600 (C=C), 1096, 1143 (C–F); ^1H NMR (400 MHz, CDCl_3 , δ , ppm): 7.50 (d, 1H, H(2), J = 16 Hz), 7.82 (d, 1H, H(3), J = 16 Hz), 8.10 (d, 2H, H(2'') and H(6'')), 6.98 (m, 2H, H(3') and H(5')), 7.11–7.66 (m, 7H, Ar–H); ^{13}C (100 MHz, CDCl_3 , δ , ppm): 189.7 (C=O), 121.6C(2), 143.7C(3), 104.7C(3'), 111.9C(5'), 159.9C(4'), 162.8C(2'), 116.1–165.4 (Ar–C); Anal. Calcd (C₂₁H₁₃F₃O): C 74.55H 3.87%. Found: C 73.63H 3.98%.

2.6.4. (2E)-1-[4-(2,4-difluorophenyl)phenyl]3-(3-methoxyphenyl)prop-2-en-1-one (10)

Pale yellow solid; Yield 98%; mp. 122–124 °C; IR (KBr, cm^{-1}): 1656 (C=O), 3062–3013 (aromatic C–H), 2934–2834 (aliphatic C–H), 1595 (C=C), 1100, 1142 (C–F); ^1H NMR (400 MHz, CDCl_3 , δ , ppm): 7.54 (d, 1H, H(2), J = 16 Hz), 7.81 (d, 1H, H(3), J = 16 Hz), 8.10 (d, 2H, H(2'') and H(6'')), 6.98 (m, 2H, H(3') and H(5')), 7.17–7.66 (m, 7H, Ar–H), 3.87 (s, 3H, OCH₃); ^{13}C (100 MHz, CDCl_3 , δ , ppm): 189.9 (C=O), 121.2C(2), 144.9C(3), 104.7C(3'), 111.9C(5'), 159.9C(4'), 162.8C(2'), 113.5–159.9 (Ar–C), 55.4 (OCH₃); mass (m/z): 351.0 [M+1]⁺; Anal. Calcd (C₂₂H₁₆F₂O₂): C 75.42H 4.60%. Found: C 74.54H 4.64%.

2.6.5. (2E)-1-[4-(2,4-difluorophenyl)phenyl]3-(2-methoxyphenyl)prop-2-en-1-one (11)

Pale yellow solid; Yield 97%; mp. 118–120 °C; IR (KBr, cm^{-1}): 1663 (C=O), 3094–3029 (aromatic C–H), 2938–2835 (aliphatic C–H), 1596 (C=C), 1108, 1143 (C–F); ^1H NMR (400 MHz, CDCl_3 , δ , ppm): 7.48 (d, 1H, H(2), J = 12 Hz), 8.16 (d, 1H, H(3), J = 16 Hz), 8.10 (d, 2H, H(2'') and H(6'')), 6.98 (m, 2H, H(3') and H(5')), 7.38–7.69 (m, 7H, Ar–H), 3.94 (s, 3H, OCH₃); ^{13}C (100 MHz, CDCl_3 , δ , ppm): 190.5 (C=O), 120.8C(2), 140.6C(3), 104.6C(3'), 111.9C(5'), 159.9C(4'), 162.8C(2'), 111.3–158.9 (Ar–C), 55.6 (OCH₃); mass (m/e): 351.0 [M+1]⁺; Anal. Calcd (C₂₂H₁₆F₂O₂): C 75.42H 4.60%. Found: C 74.25H 4.62%.

2.6.6. (2E)-1-[4-(2,4-difluorophenyl)phenyl]3-(thiophenyl)prop-2-en-1-one (12)

Pale yellow solid; Yield 92%; mp. 120–122 °C; IR (KBr, cm^{-1}): 1654 (C=O), 3108–3039 (aromatic C–H), 2922–2851 (aliphatic C–H), 1588 (C=C), 1099, 1137 (C–F); ^1H NMR (400 MHz, CDCl_3 , δ , ppm): 7.49 (d, 1H, H(2), J = 12 Hz), 7.99 (d, 1H, H(3), J = 16 Hz), 8.09 (d, 2H, H(2'') and H(6'')), 6.98 (m, 2H, H(3') and H(5')), 7.11–7.65 (m, 6H, Ar–H); ^{13}C (100 MHz, CDCl_3 , δ , ppm): 189.3 (C=O), 120.6C(2), 140.4C(3), 104.7C(3'), 111.9C(5'), 159.9C(4'), 162.8C(2'), 124.3–139.4 (Ar–C); mass (m/z): 327.1 [M+1]⁺; Anal. Calcd (C₁₉H₁₂F₂OS): C 69.92H 3.71 S 9.83%. Found: C 67.16H 3.68 S 9.28%.

2.6.7. (2E)-1-[4-(2,4-difluorophenyl)phenyl]3-(naphthyl)prop-2-en-1-one (13)

Yellow solid; Yield 56%; m.p. 104–106 °C; IR (KBr, cm^{-1}): 1654 (C=O), 3045–3007 (aromatic C–H), 2922–2849 (aliphatic C–H), 1592 (C=C), 1098, 1143 (C–F); ^1H NMR (400 MHz, CDCl_3 , δ , ppm): 7.60 (d, 1H, H(2), J = 16 Hz), 8.72 (d, 1H, H(3), J = 16 Hz), 8.17 (d, 2H, H(2'') and H(6'')), 6.97 (m, 2H, H(3') and H(5')), 7.47–8.29 (m, 10H, Ar–H); ^{13}C (100 MHz, CDCl_3 , δ , ppm): 189.7 (C=O), 124.9C(2), 141.9C(3), 104.7C(3'), 111.9C(5'), 159.9C(4'), 162.8C(2'), 123.5–139.5 (Ar–C); mass (m/z): 371.1 [M + 1]⁺; Anal. Calcd (C₂₅H₁₆F₂O): C 81.07H 4.35%. Found: C 78.57H 4.33%.

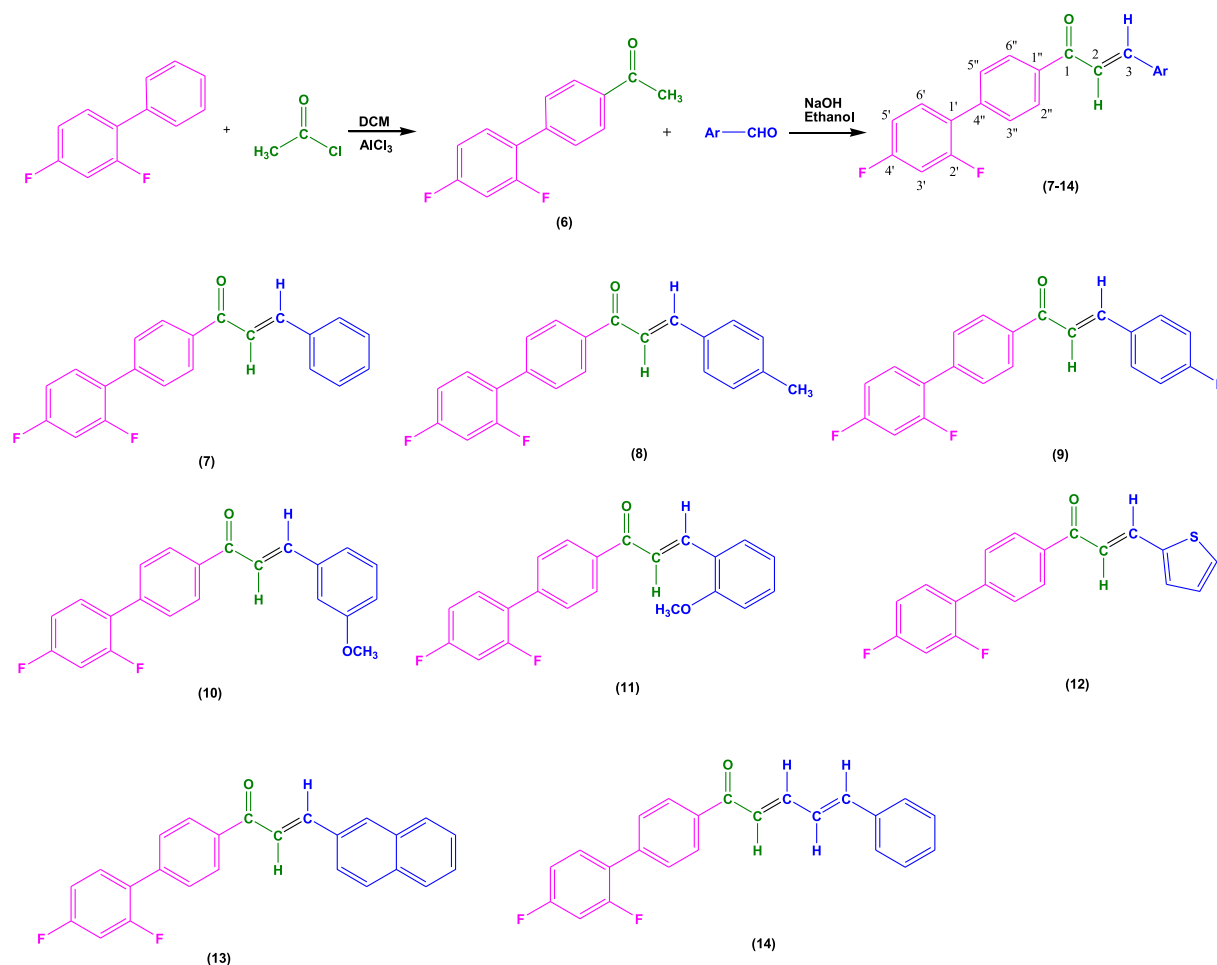
2.6.8. (2E)-1-[4-(2,4-difluorophenyl)phenyl]3-(cinnamyl)prop-2-en-1-one (14)

Pale yellow solid; Yield 84%; m.p. 124–126 °C; IR (KBr, cm^{-1}): 1650 (C=O), 3080–3024 (aromatic C–H), 2922–2857 (aliphatic C–H), 1579 (C=C), 1099, 1140 (C–F); ^1H NMR (400 MHz, CDCl_3 , δ , ppm): 7.14 (d, 1H, H(2), J = 16 Hz), 7.66 (d, 1H, H(3), J = 12 Hz), 8.06 (d, 2H, H(2'') and H(6'')), 6.97 (m, 2H, H(3') and H(5')), 7.05–7.67 (m, 10H, Ar–H); ^{13}C (100 MHz, CDCl_3 , δ , ppm): 189.9 (C=O), 125.3C(2), 145.1C(3), 104.7C(3'), 111.9C(5'), 159.9C(4'), 162.8C(2'), 125.3–142.2 (Ar–C); Anal. Calcd (C₂₃H₁₆F₂O): C 79.75H 4.66%. Found: C 79.52H 4.84%.

3. Results and discussion

The schematic representation of synthesizing the biphenyl based difluoro-chalcones starting from 2',4'-difluorobiphenyl has been described in Scheme 1. The 2',4'-difluorobiphenyl has been made to undergo Friedel–Crafts acylation reaction with acetylchloride in the presence of dichloromethane and aluminium chloride to synthesize 1-(2',4'-difluorobiphenyl-4-yl)ethanone (6) also reported in Ref. [25]. A series of (2E)-1-[4-(2,4-difluorophenyl)phenyl]3-arylprop-2-en-1-ones (7–14) have been synthesized by the Claisen-Schmidt condensation method with excellent yield. All the synthesized compounds (7–14) have been characterized by elemental analysis, FT-IR, ^1H and ^{13}C NMR and Mass spectroscopy.

The mass spectra of the compounds exhibit [M+1]⁺ peaks which confirms the formation of product. The numbering of the carbon atoms was displayed in Scheme 1 and the protons are



Scheme 1. Schematic representation of synthesis of difluorobiphenyl chalcones (7–14).

Table 1

Crystal data and structure refinement details.

CCDC number	CCDC 1060166
Empirical formula	C ₂₁ H ₁₄ F ₂ O
Formula weight	320.32
Temperature	296(2) K
Wavelength	0.71073 Å
Crystal system	Triclinic
Space group	P1
Unit cell dimensions	a = 6.2485(9) Å; α = 86.190(8)° b = 7.7232(10) Å; β = 86.140(8)° c = 16.4261(17) Å; γ = 84.828(9)° 786.22(17) Å ³
Volume	786.22(17) Å ³
Z	2
Density (calculated)	1.353 Mg/m ³
Absorption coefficient	0.098 mm ⁻¹
F(000)	332
Crystal size	0.25 × 0.22 × 0.16 mm ³
Theta range for data collection	2.490–25.889°
Index ranges	–7 ≤ h ≤ 7, –9 ≤ k ≤ 9, –19 ≤ l ≤ 20
Reflections collected	3262
Independent reflections	2022 [R(int) = 0.0187]
Completeness to theta = 25.000°	66.8%
Refinement method	Full-matrix least-squares on F ²
Data/restraints/parameters	2022/0/217
Goodness-of-fit on F ²	1.033
Final R indices [I > 2σ(I)]	R1 = 5.7%, wR2 = 14.2%
R indices (all data)	R1 = 8.6%, wR2 = 16.9%
Largest diff. peak and hole	0.171 and –0.206 e.Å ⁻³

numbered accordingly. The discussion about IR and NMR (¹H, ¹³C, ¹⁹F and ¹H – ¹³C COSY) spectra were made with the representative compound **7**.

3.1. IR spectral analysis

In our present study, the absorption band around 1666 cm⁻¹ indicates the presence of C=O group of chalcone. The aliphatic C=C stretching frequency observed at 1597 cm⁻¹. A collection of bands in the range of 3094–3021 cm⁻¹ and 2924–2855 cm⁻¹ were due to aromatic C–H stretching and aliphatic C–H stretching respectively. The stretching frequency around 1090–1140 cm⁻¹ corresponds to the C–F stretching vibration.

3.2. NMR spectral analysis

The ¹H NMR spectra has been assigned depending upon their integrals, positions and multiplicities. The two doublets observed at 7.57 ppm (J = 16 Hz) and 7.85 ppm (J = 16 Hz) corresponds to one proton each were due to the olefinic protons [H(2) and H(3)] which reveals the formation of the chalcone. The observation of large (J = 16 Hz) coupling constant clearly indicated the formation of (*E*)-isomer which was more stable compared to the (*Z*)-isomer. Hence, all the compounds (**7–14**) exist in the *trans* form (*i.e.*) as (*E*)-isomer due to their higher stability. A doublet at 8.10 ppm with integral value of two was due to the protons [H(2'') and H(6'')] ortho to the carbonyl group. The carbonyl group bearing more electronegative

Table 2
Geometric details of hydrogen bond (\AA , $^\circ$) for compound 7 (D-donor; A-acceptor; H-hydrogen).

Interactions	D-H	H ... A	D ... A	D-H ... A	Symmetry
C12-H12 ... F1	0.93	2.46	2.900(4)	109 $^\circ$	x, y, z
C15-H15 ... O1	0.93	2.47	2.796(4)	101 $^\circ$	
C8-H8 ... F1	0.93	2.43	3.352(4)	173 $^\circ$	x-1,y,z
C2-H2 ... Cg1 ^a	0.93	2.88	3.571(4)	132 $^\circ$	-x,1-y,1-z
Cg2 ^b ... Cg2 ^b			3.877(2)		-1-x,1-y,1-z

^a Cg1 denotes centroid of the phenyl ring (C16/C17/C18/C19/C20/C21).

^b Cg2 denotes centroid of the phenyl ring (C7/C8/C9/C10/C11/C12).

oxygen atom shifts the adjacent protons towards downfield. The multiplet at 6.97 ppm is assigned to the protons [H(3') and H(5')] adjacent to the fluorine substituted carbon atoms. The remaining signals in the range of 7.43–7.66 ppm were characteristic of the aromatic protons.

The ^{13}C spectrum of fluorine substituted compounds found to be little complex due to carbon–fluorine coupling. In the ^{13}C NMR spectra, the signal around 189.9 ppm clearly explained the presence of carbonyl carbon C(1). The sharp peaks at 121.9 and 145.1 ppm were corresponding to olefinic carbons C(2) and C(3) respectively. The signals around 104.7 and 111.9 ppm were due to the C(3') and C(5') respectively. The low intense signals resonate at 124.3C(1'), 134.9C(1''), 137.3C(1''') and 139.4C(4'') ppm were respective to *ipso* carbons. The less intense peaks appeared as double doublets around 159.9C(2') and 162.8C(4') ppm were due to fluorine substituted carbon atoms. The coupling constant $^1J_{\text{C-F}}$ was found to be 249 Hz for C(2') and 250 Hz for C(4') which is in close proximity to the standard value ($^1J_{\text{C-F}} = 250$ Hz).

Generally, the presence of fluorine atom undergoes long range coupling with the neighbouring atoms. Fluorine is an atom of small size, having spin $\frac{1}{2}$ and exist as ^{19}F with 100% natural abundance. The long range NMR spin–spin coupling constant of ^{19}F is an important

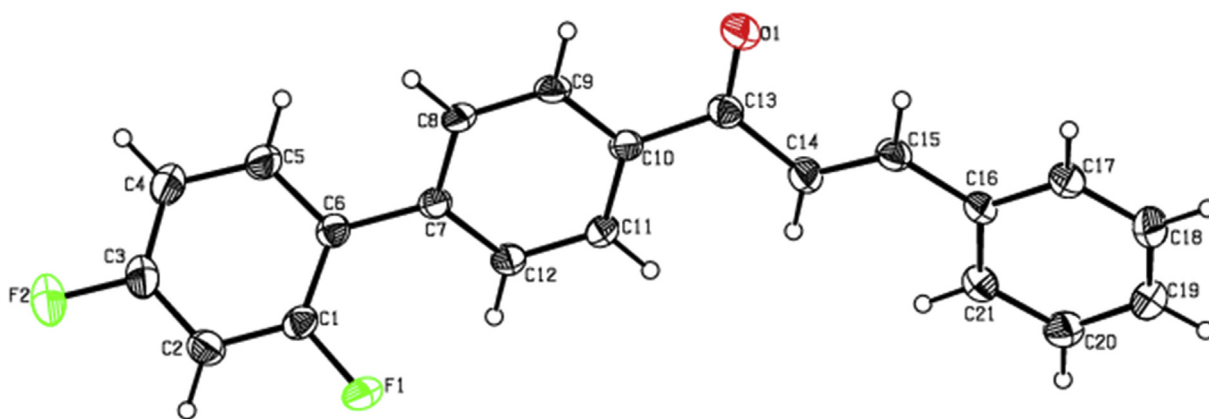


Fig. 2. ORTEP of compound 7.

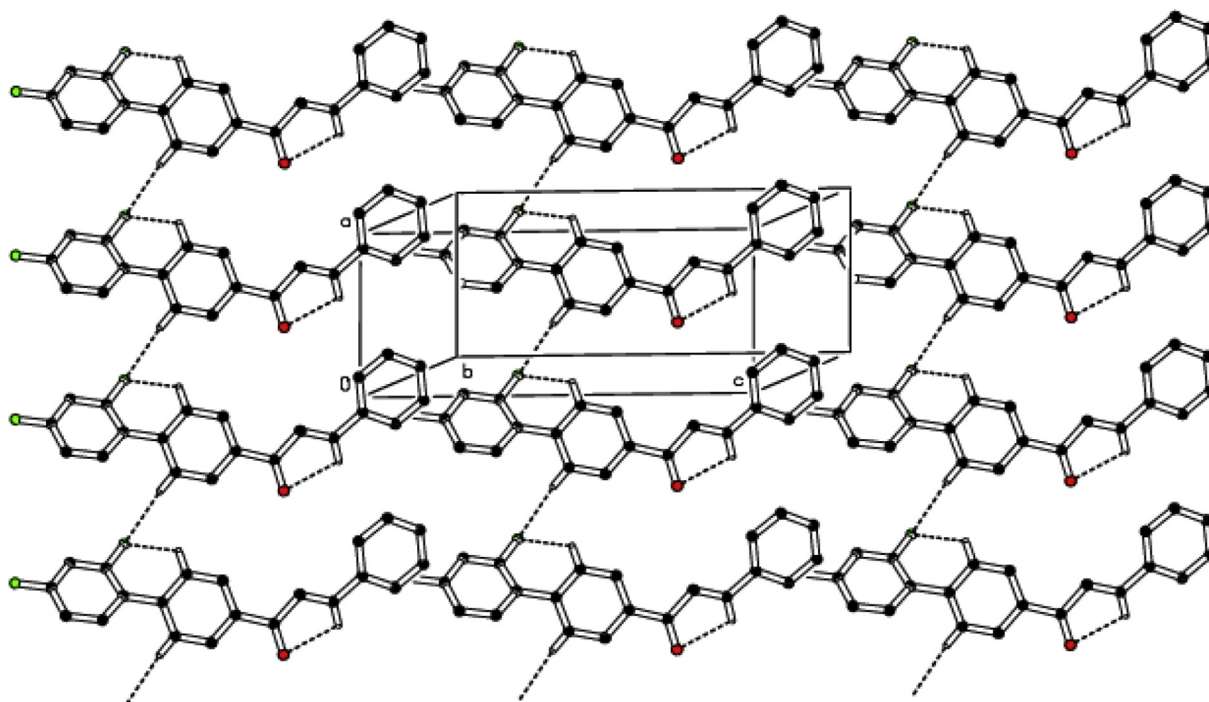


Fig. 3. Molecular packing of the title compound, viewed down the *b* axis; Intramolecular C–H...F, C–H...O and intermolecular C–H...F hydrogen bonds are shown as dashed lines. For the sake of clarity, H atoms, not involved in hydrogen bonds, have been omitted for clarity.

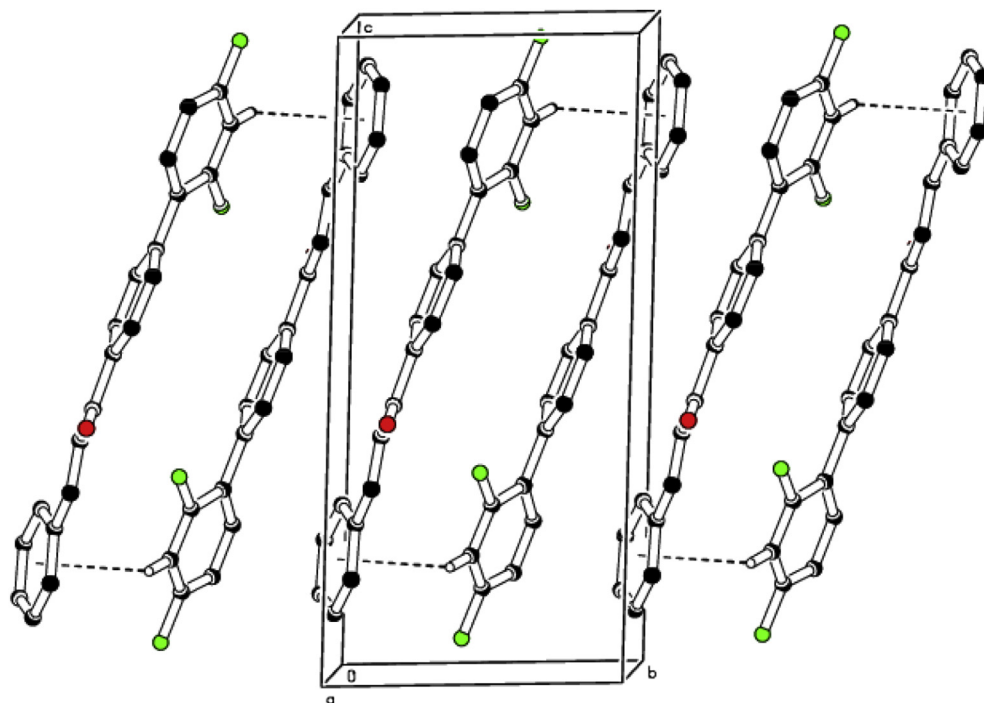


Fig. 4. Molecular packing of the title compound, viewed along the *a* axis; Intermolecular C–H... π interactions are shown as dashed lines. For the sake of clarity, H atoms, not involved in hydrogen bonds, have been omitted for clarity.

parameter for studying the structure of polycyclic aliphatic carbons, steroids and aromatic molecules. The ^{19}F spectrum displays two doublets in the range of -112.86 ppm ($J = 7.52$ Hz) and -109.84 ppm ($J = 7.52$ Hz) each corresponding to one fluorine concluded the presence of two fluorine atoms in the compound.

The 2D-NMR spectroscopy is a tool for assigning the ^1H and ^{13}C spectra without any discrepancies. The tentative assignment made

from the results of ^1H and ^{13}C are verified and reassured by the two dimensional NMR spectroscopy. In the ^1H – ^{13}C COSY spectrum, the correlation at 121.9 with proton 7.55 ppm H(2) is assigned for C(2) carbon, while the signal at 145.1 correlated with proton 7.83 ppm H(3) is attributed to C(3). This confirms the formation of the expected product. In addition, there are other correlations between ^1H and ^{13}C which concludes the assignment of structure (Table S1).

3.2.1. X-ray structure analysis of 1-[4-(2,4-difluorophenyl)phenyl] 3-phenylprop-2-en-1-one (7)

The single crystal measurements of compound 7 reveals that it crystallizes in a triclinic system with $P\bar{1}$ space group. Table 1 summarizes the crystal data, intensity data collection and refinement details for the compound 7. The hydrogen bonds involved in the structure were presented in Table 2 and the atomic coordinates of the non-hydrogen atoms with their equivalent temperature factors were listed in Table S2.

The ORTEP structure of the molecule drawn at 30% probability thermal displacement ellipsoids with the atom numbering scheme was shown in Fig. 2. All the bond distances and bond angles are agreed with the reported literature values. The bond length C13–O1 confirms the double bond character. The widening of C11–C10–C13 bond angle [124.2 (3°)] is due to the short contact H11...H14 (2.1 Å).

Fluorine atoms F1 and F2 deviate -0.009 (1) and -0.005 (1) Å, respectively from the attached phenyl ring. The dihedral angle between fluoro phenyl ring and its attached (central) phenyl ring is 37.4 (1°). Fluoro phenyl ring and the outer phenyl ring is oriented with a dihedral angle of 48.5 (1°).

In addition to van der Waals interactions, the molecular structure is influenced by C–H...F and C–H...O intramolecular hydrogen bonds. Intermolecular C–H...F hydrogen bonds stabilize the molecular packing. This intermolecular hydrogen bond forms a C(6) chain-like arrangement along [101] plane in the unit cell (Fig. 3). Atom H2 forms a C–H... π intermolecular interaction with

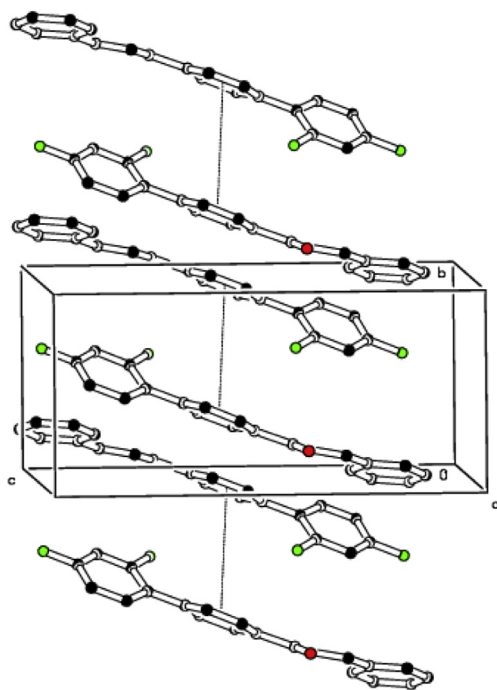


Fig. 5. Molecular packing of the title compound, viewed along the *a* axis; Intermolecular π ... π interactions are shown as dashed lines. For the sake of clarity, H atoms, not involved in hydrogen bonds, have been omitted for clarity.

Table 3
Selected geometric parameters [bondlengths (Å), bond angles (°) and torsional angles (°)] for compound 7.

Atoms	Bond length		Atoms	Bond angle		Atoms	Torsional angle	
	XRD	Theoretical		XRD	Theoretical		XRD	Theoretical
O1-C13	1.218(4)	1.229	F1-C1-C2	116.4(3)	117.1	F1-C1-C2-C3	179.6(4)	179.3
F1-C1	1.352(3)	1.349	F1-C1-C6	119.6(3)	119.5	C1-C2-C3-F2	-179.6(4)	-179.8
F2-C3	1.362(4)	1.346	C2-C1-C6	123.9(3)	123.4	F2-C3-C4-C5	179.5	179.8
C1-C2	1.371(4)	1.389	C3-C2-C1	117.3(3)	117.8	C2-C1-C6-C5	0.8(6)	0.16
C1-C6	1.382(5)	1.403	F2-C3-C4	118.7(3)	119.3	F1-C1-C6-C5	-179.4(3)	179.3
C2-C3	1.364(5)	1.389	F2-C3-C2	118.4(4)	118.7	C2-C1-C6-C7	178.7(3)	-179.2
C3-C4	1.359(5)	1.390	C4-C3-C2	122.9(3)	121.9	C6-C7-C8-C9	-178.3	-178.4
C4-C5	1.385(5)	1.392	C3-C4-C5	118.0(3)	118.4	C11-C10-C13-O1	173.2(3)	-178.7
C5-C6	1.395(4)	1.407	C4-C5-C6	122.3(3)	122.5	O1-C13-C14-C15	12.1(5)	9.7
C6-C7	1.489(4)	1.484	C1-C6-C5	115.6(3)	116.0			
C7-C8	1.391(5)	1.408	C1-C6-C7	123.9(3)	122.9			
C7-C12	1.398(4)	1.405	C5-C6-C7	120.5(3)	121.1			
C8-C9	1.384(4)	1.388	C8-C7-C12	117.9(3)	118.1			
C9-C10	1.393(4)	1.403	C8-C7-C6	119.7(3)	121.9			
C10-C11	1.384(5)	1.402	C12-C7-C6	122.4(3)	119.9			
C10-C13	1.495(4)	1.501	C9-C8-C7	121.1(3)	120.8			
C11-C12	1.384(4)	1.393	C8-C9-C10	120.8(3)	120.9			
C13-C14	1.481(5)	1.482	C11-C10-C9	118.3(3)	118.5			
C14-C15	1.325(4)	1.349	C11-C10-C13	124.1(3)	123.4			
C15-C16	1.470(4)	1.466	C9-C10-C13	117.6(3)	117.9			
C16-C21	1.387(5)	1.407	C12-C11-C10	121.1(3)	120.5			
C16-C17	1.393(5)	1.408	C11-C12-C7	120.8(4)	121.1			
C17-C18	1.391(5)	1.391	O1-C13-C14	120.8(3)	118.8			
C18-C19	1.355(6)	1.399	O1-C13-C10	120.1(3)	119.8			
C19-C20	1.382(5)	1.395	C14-C13-C10	119.1(3)	121.4			
C20-C21	1.390(5)	1.393	C15-C14-C13	120.9(4)	121.3			
			C14-C15-C16	127.1(4)	127.2			
			C21-C16-C17	118.2(3)	118.1			
			C21-C16-C15	122.2(3)	118.5			
			C17-C16-C15	119.6(4)	123.2			
			C18-C17-C16	120.4(4)	120.7			
			C19-C18-C17	120.8(4)	120.4			
			C18-C19-C20	119.9(4)	119.6			
			C19-C20-C21	120.0(4)	119.9			
			C16-C21-C20	120.7(3)	121.1			

the centroid (Cg1) of phenyl ring (C16/C17/C18/C19/C20/C21) at $(-x, 1-y, 1-z)$ with an H2-Cg1 separation of 2.88 Å (Fig. 4). In addition to this intermolecular $\pi \dots \pi$ stacking interactions is also observed between the centroids of the phenyl ring (C7/C8/C9/C10/C11/C12) at $(-1-x, 1-y, 1-z)$ with a centroid-centroid distance of 3.877(2) Å (Fig. 5).

3.3. Theoretical calculations

The molecular geometry was optimized using Density Functional Theory (DFT/B3LYP) method with 6-31G(d,p) basis set. The optimized structure and geometrical parameters of compound 7

were derived and compared with the XRD values (Table 3). The optimized molecular geometry of compound 7 was displayed in Fig. 6. The theoretical bond lengths were closer to the experimental values. For the bond angle and torsional angle the maximum deviation was found to be 3.7°. The deviations may result because the theoretical calculations belong to the gaseous phase and the experimental results belong to the solid phase.

3.3.1. HOMO-LUMO analysis

The highest occupied molecular orbital (HOMO) and lowest unoccupied molecular orbital (LUMO) are termed as frontier molecular orbitals (FMOs) which play a major role in the optical and

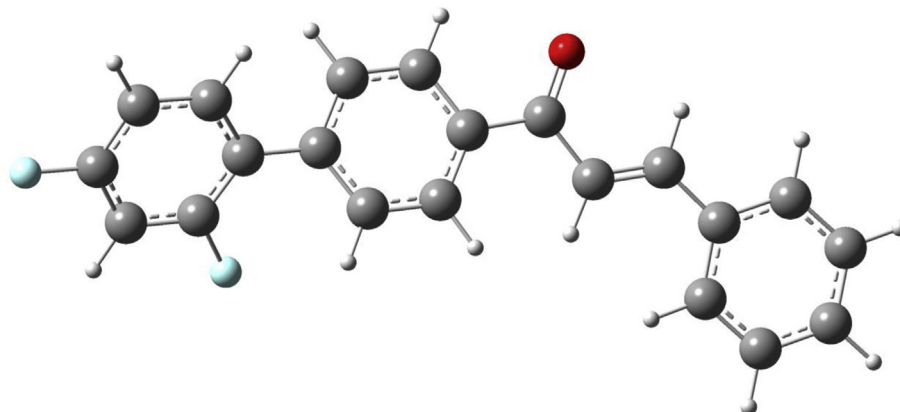


Fig. 6. Optimized molecular structure of compound 7.

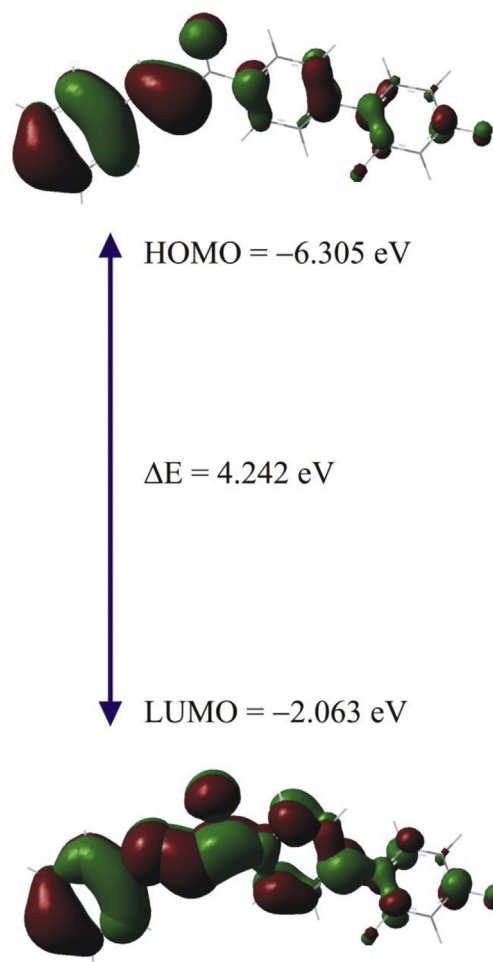


Fig. 7. HOMO-LUMO energy gap of compound 7.

electrical properties as well as in quantum chemistry [26]. It is an important tool to find the transition of electron from ground state to excited state. The chemical reactivity descriptors like chemical potential (μ), global hardness (η) and softness (ζ), electrophilicity index (ω) and electronegativity (χ) which are derived from HOMO and LUMO are helpful in understanding the ecotoxicological characteristics of the drug molecules and various aspects in the drug design [27]. In our present study, the E_{HOMO} and E_{LUMO} were -6.305 eV and -2.063 eV respectively. The HOMO-LUMO plot was shown in Fig. 7 and the energy separation ($\Delta E = E_{\text{HOMO}} - E_{\text{LUMO}}$) was found to be 4.242 eV. This large frontier energy gap suggested that the compound was less polarizable with low chemical reactivity and high kinetic stability [28]. The chemical reactivity

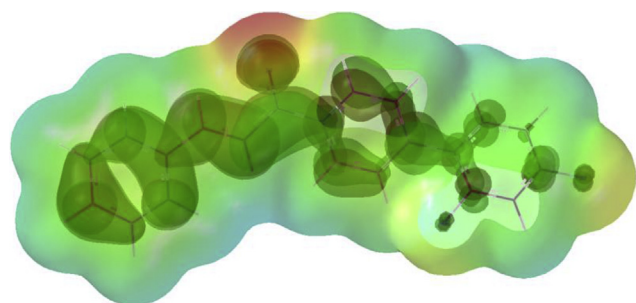


Fig. 8. MEP diagram of compound 7.

descriptors were calculated from the following expressions,

$$\text{Chemical potential, } \mu = E_{\text{HOMO}} + E_{\text{LUMO}}/2 = -4.185 \text{ eV}$$

$$\text{Global hardness, } \eta = E_{\text{LUMO}} - E_{\text{HOMO}}/2 = 2.119 \text{ eV}$$

$$\text{Global Softness, } \zeta = 1/2\eta = 0.236 \text{ eV}$$

$$\text{Electrophilicity index, } \omega = \mu^2/2\eta = 4.133 \text{ eV}$$

$$\text{Electronegativity, } \chi = -\mu = 4.185 \text{ eV}$$

The electrophilicity index was used to measure the stabilization in energy when the system gained an additional electronic charge from the environment. The chemical potential of the compound was found to be negative which concluded that it was stable and did not decompose spontaneously. The value of hardness and softness revealed that the compound was hard with less polarizability.

3.3.2. Molecular electrostatic potential (MEP)

Molecular electrostatic potential (MEP) generally allows to visualize variably charged regions of a molecule in terms of color grading. It was calculated to predict the electrophilic and

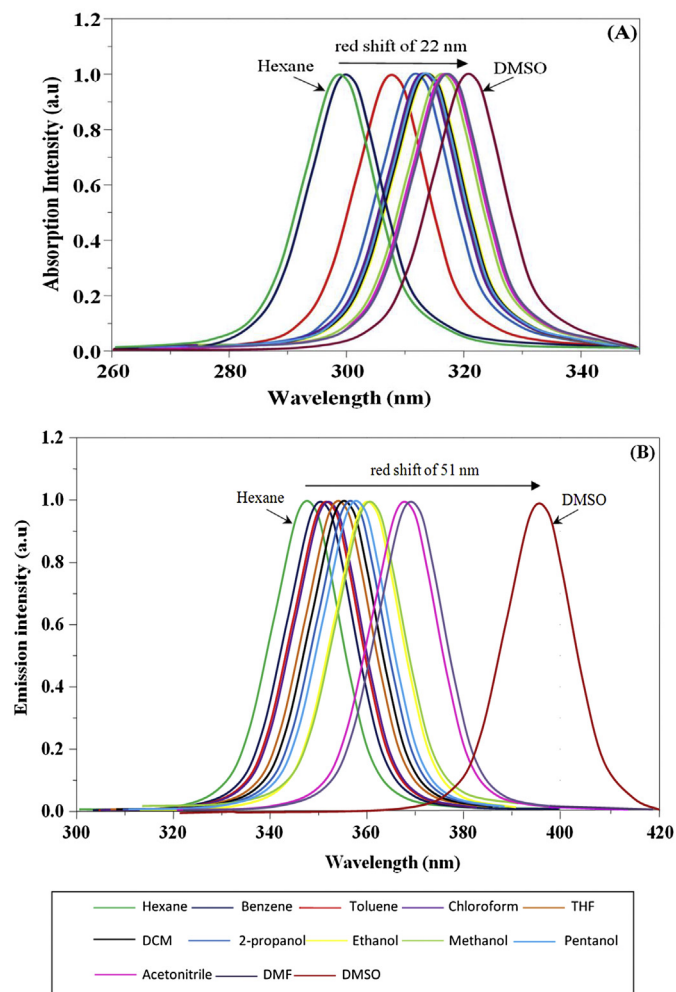


Fig. 9. Normalized absorption (A) and emission (B) spectrum of compound 7 in different solvents.

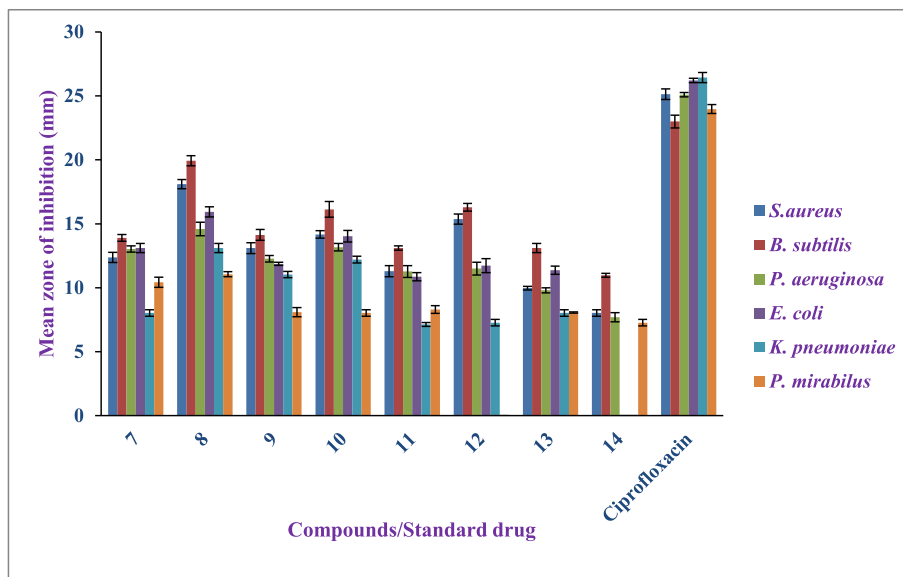


Fig. 10. Antibacterial activities of compounds 7–14 by disc diffusion method.

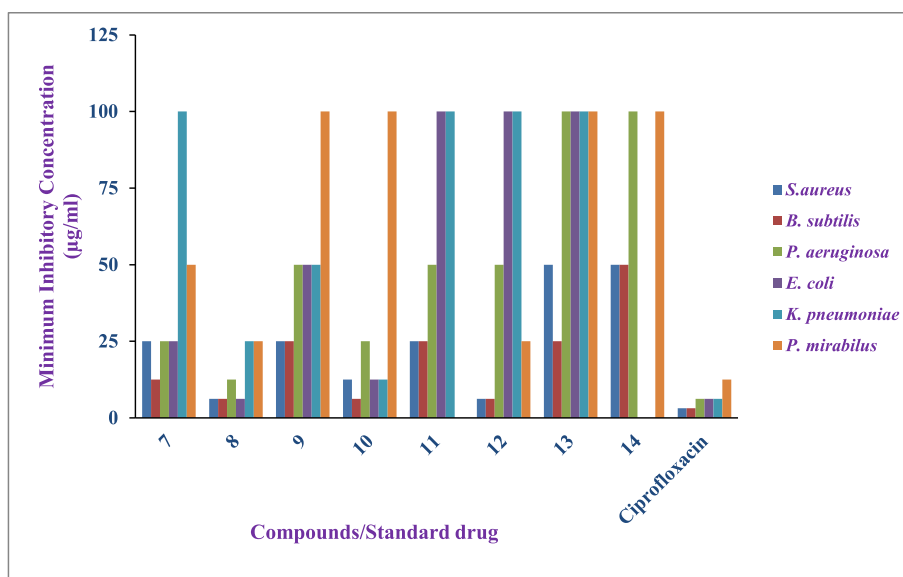


Fig. 11. Antibacterial activities of compounds 7–14 by twofold serial dilution method.

nucleophilic attack of the molecule under study. The 3D electrostatic potential map of the compound **7** was shown in Fig. 8. The order of electrostatic potential exist as red < orange < yellow < green < blue (in web version). The blue corresponds to highest electrostatic potential energy and the red corresponds to lowest electrostatic potential energy. From the map, we concluded that the carbonyl group undergo electrophilic attack and have the lowest electrostatic potential whereas the other regions represent the intermediary electrostatic potentials.

3.4. Solvatochromism

The solvatochromic behavior of compound **7** have been investigated with 13 solvents of varying polarity. The solvent can considerably influence the chemical and physical properties of the solute. The electronic transitions of solutes in different solvents (solvatochromism) were based on the nature and the extent of the solute–solvent interactions in the ground and first excited states of solutes [29]. The absorption and fluorescence spectra of **7** were

Table 4
Docking score of the compounds (7–14).

Compound	7	8	9	10	11	12	13	14	
G score	−10.0	−10.5	−10.5	−10.3	−11.0	−10.4	−9.7	−10.0	
Interacting residues	TRP 171, TYR 85, PHE 62, TRP 140	TRP 171, TRP 102, TYR 60, PHE 62, TRP 140	TRP 171, TRP 102, TYR 60, PHE 62, HIE 135, TRP 140	TRP 171, TYR 85, HIE 135	TRP 171, TYR 60, PHE 62, HIE 135, ARG 103	TRP 171, TYR 85, TRP 140, TYR 140, TRP 102, PHE 62	TRP 171, TYR 60, TRP 140, TRP 102, PHE 62	TRP 171, HIE 135	TRP 140, HIE 135

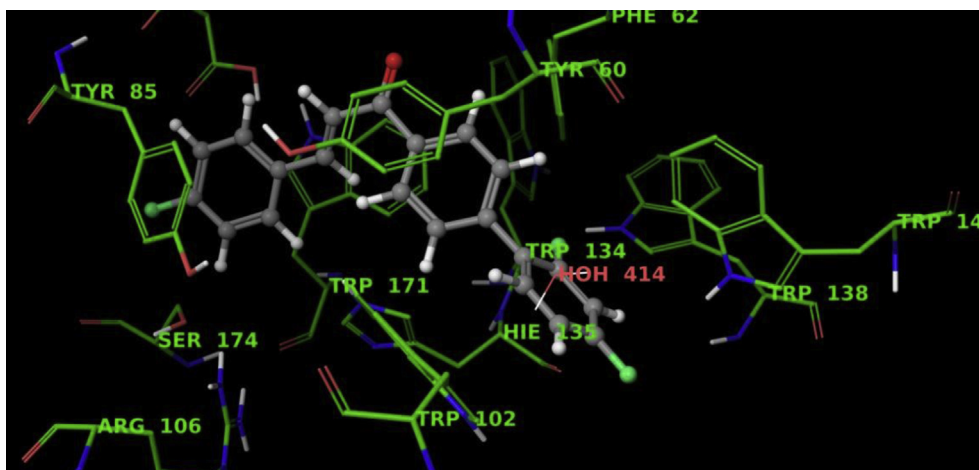


Fig. 12. Molecular docking studies of compound **9** with 4LRH.

displayed in Fig. 9(A) and (B) respectively and their corresponding spectral data are summarized in Table S3. The absorption band between 299 and 321 nm in different solvents has been assigned to π - π^* transition.

As the polarity of the solvent increased from non-polar solvent (hexane) to polar solvent (Dimethylsulfoxide-DMSO) there was a substantial increase in the absorption maxima indicating a bathochromic shift (positive solvatochromism). An appreciable red shift of 22 nm in the absorption by solvation represents that the first excited state was more stabilized relative to that of the ground state [30]. The emission spectra displayed an appreciable bathochromic shift when the polarity of the solvent increased and there was a broad band from 347 to 398 nm on excitation at 300 nm. This was due to the fact that the highly dipolar excited state in polar solvents was more stabilized. A dramatic red shift of 51 nm was observed in the emission spectra on going from hexane to DMSO because of the intramolecular charge transfer in the singlet excited state.

3.5. Antimicrobial evaluation

The compounds (**7–14**) were screened for *in vitro* antimicrobial activity against gram-positive bacteria (*B. subtilis* and *S. aureus*) and gram-negative bacteria (*P. aeruginosa*, *E. coli*, *K. pneumoniae* and *Proteus mirabilis*). The mean zone of inhibition produced by the compounds (**7–14**) in agar diffusion methods against tested bacterial strains ranged from 7 to 19 mm. The negative control (50%

DMSO) did not produce zone of inhibition for all the bacterial strains tested. Ciprofloxacin (5 μ g/disc) was used as antibacterial positive control and it produced mean zone of inhibition ranged between 23 and 26 mm. In our study the gram-positive bacteria were more susceptible than the gram-negative bacteria.

It is very interesting to observe that the antimicrobial activities depend upon the nature (electron releasing and electron withdrawing) and position of the substituent in the phenyl ring. It is evident from Fig. 10 that excellent activity was shown by compound **8** with electron releasing substituent ($-\text{CH}_3$) against gram-positive bacteria. However, there was a moderate to good activities exhibited against the gram-positive and gram-negative bacteria for all the remaining compounds. In addition, the halogen substituted compound **9** displays moderate activities and the compound **14** exhibits very weak activities against antibacterial strains. The compound **10** with methoxy group at *meta* position shows better antibacterial activity compared to compound **11** with methoxy group at *ortho* position.

The Minimum Inhibitory Concentration (MIC) values of the tested compounds were displayed in Fig. 11. The observation of the results revealed that the compounds **8**, **10** and **12** have more pronounced antibacterial activities. The compound **8** with 4-methyl substituted aromatic ring has shown significant MIC values against *S. aureus*, *B. subtilis*, and *E. coli*. The 2-thiophenyl substituted compound **12** was potent against *S. aureus*, *B. subtilis* and the 3-methoxy substituted compound **10** was active against *B. subtilis*.

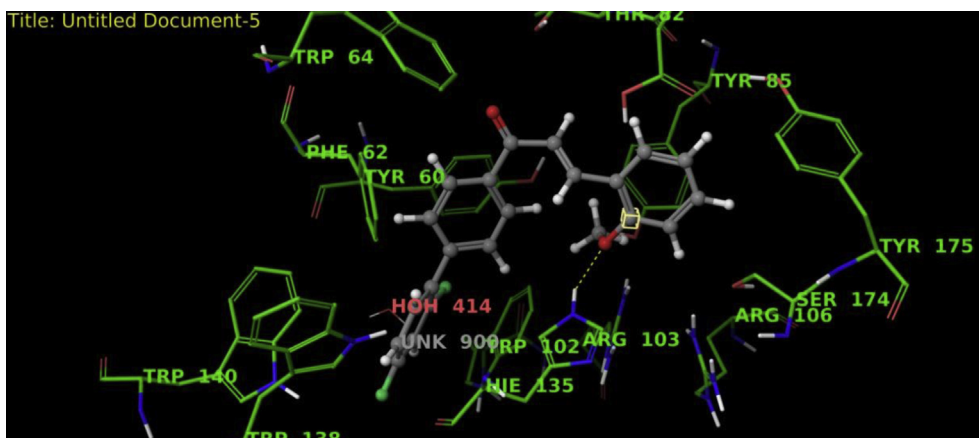


Fig. 13. Molecular docking studies of compound **11** with 4LRH.

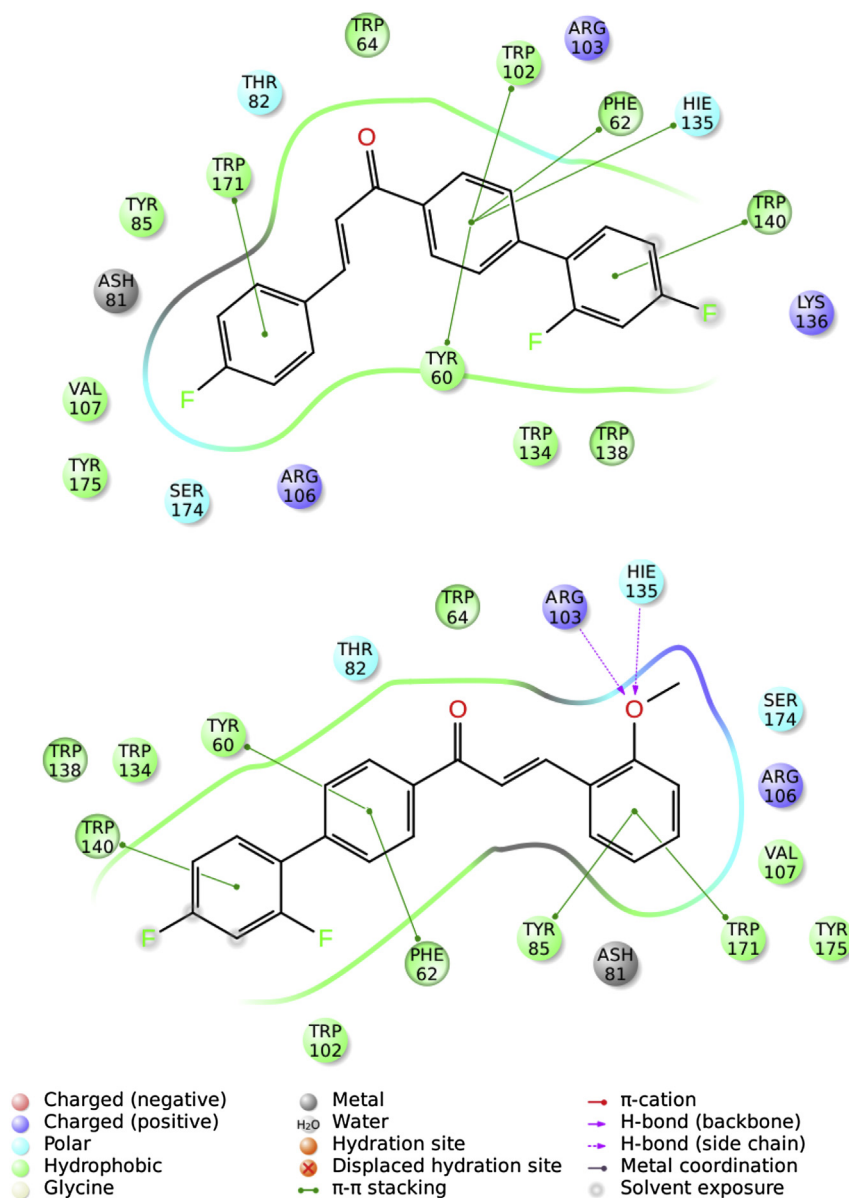


Fig. 14. 2-D images of Molecular docking studies of compound **9** and **11** with 4LRH protein residues.

The other compounds exhibit only moderate antibacterial activities.

From the above discussion it is clear that the antimicrobial screening of compounds (**7–14**) shows better activity toward gram-positive bacteria than gram-negative bacteria. The compound **8** exhibits superior activity over others against all the tested organisms.

3.6. Molecular docking studies

It is a challenge to medicinal chemists to discover a new drug in minimum cost and time. Thereby to enable this need advanced computational standard technique like molecular docking studies is helpful in reducing the cost and time of drug discovery. It is an emerging technique to gain an insight into the exact binding location of the ligand and protein [31].

In order to analyze the anticancer activity, the synthesized ligands (**7–14**) were subjected to molecular docking using the crystal structure of human folate receptor alpha in complex with folic acid

(PDB ID: 4LRH). The folate receptors ($FR\alpha$) are cysteine rich glycoproteins which are used for the development of many cancer therapeutics, high affinity anti-folates and folate conjugated drugs and toxins. Therefore, the $FR\alpha$ – folic acid complex structure becomes an important target for receptor mediated chemotherapy [32].

The efficiency of the ligands to bind with the target protein was evaluated by G score (Table 4). The G score is an empirical function that includes many factors like hydrophobicity, hydrogen bonding, rotation penalty etc. The docked ligands were ranked based on various types of interactions between the ligand and protein. The results revealed that all ligands were found to accommodate the active pocket of the receptor and showed excellent G score ranging from -11.0 to -9.7 . Among the docked compounds, **11** was found to be most potent with the score of -11.0 . The 3D and 2D binding mode of the compounds **9** and **11** were displayed in Figs. 12–14. It was observed that the compound **11** had hydrogen bond interaction with positively charged ARG103 and polar group HIE135. The compounds **7–12** showed significant π - π stacking interactions

with hydrophobic residues TRP171, TYR85, TRP102, TYR60, TRP140 and PHE62. The difluoro substituted aromatic ring in all the compounds except **10** and **13** had interaction with the hydrophobic residue TRP140. It is evident that, the compounds **7**, **14** show moderate and **13** have high G score compared to other ligands. The results furnished that the compounds with 4-methyl, 4-fluoro, and 2-methoxy substituted chalcones have competency to inhibit 4LRH protein and thus have high potential to act as anticancer agents.

4. Conclusions

In conclusion, we have synthesized a series of novel (2E)-1-[4-(2,4-difluorophenyl)phenyl]3-arylprop-2-en-1-ones and single crystal XRD analysis were made for compound **7**. The optimized geometrical parameters were in good correlation with the experimental results. Studies with solvents of varying polarity showed positive solvatochromism. From the antibacterial study we ascertain that the compound **8** exhibit potent inhibitory activity over the others. The observations from the molecular docking simulations helped to understand the binding mode of the compounds with the target protein. The docking results showed that compound **11** has more proficiency to bind with the receptor. Further, a wide range of novel derivatives, investigations and applications of difluorobiphenyl chalcones are being carried out in our laboratory and our findings offers a good start point for drug discovery.

Acknowledgement

We express our sincere thanks to Department of Chemistry, Annamalai University, Annamalaiagar, Tamilnadu for providing laboratory and library facilities.

Appendix A. Supplementary data

Supplementary data related to this article can be found at <http://dx.doi.org/10.1016/j.molstruc.2015.06.078>.

References

- [1] M. Giulia, M. Luisa, F. Paola, S. Silvia, R. Angelo, M. Luisa, B. Francesco, L. Roberta, M. Chiara, M. Valeria, L.C. Paolo, T. Elena, *Bioorg. Med. Chem.* 12 (2004) 5465.
- [2] M. Funakoshi-Tago, K. Nakamura, R. Tsuruya, M. Hatanaka, T. Mashino, Y. Sonoda, T. Kasahara, *Int. Immunopharmacol.* 10 (2010) 562–571.
- [3] Z. Nowakowska, *Eur. J. Med. Chem.* 42 (2007) 125–137.
- [4] A. Agarwal, K. Srivastava, S.K. Puri, P.M.S. Chauhan, *Bioorg. Med. Chem. Lett.* 15 (2005) 3133–3136.
- [5] P.M. Sivakumar, S. Ganesan, P. Veluchamy, M. Doble, *Chem. Biol. Drug. Des.* 76 (2010) 407–411.
- [6] J.C. Aponte, M. Verastegui, E. Malaga, M. Zimic, M. Quiliano, A.J. Vaisberg, R.H. Gilman, G.B. Hammond, *J. Med. Chem.* 51 (2008) 6230–6234.
- [7] A. Shah, A. Khan, R. Qureshi, F. Ansari, M. Nazar, S. Shah, *Int. J. Mol. Sci.* 9 (2008) 1424–1434.
- [8] J. Quintin, J. Desrivot, S. Thoret, P.L. Menez, T. Cresteil, G. Lewin, *Bio. Org. Med. Chem. Lett.* 19 (2009) 167–169.
- [9] (a) S.K. Kumar, E. Hager, C. Petti, H. Gurulingppa, N.E. Davidson, S.R. Khan, *J. Med. Chem.* 46 (2003) 2813–2815; (b) J.R. Dimmock, D.W. Elias, M.A. Beazely, N.M. Kandepu, *Curr. Med. Chem.* 6 (1999) 1125–1149.
- [10] J.H. Wu, X.H. Wang, Y.H. Yi, K.H. Lee, *Bio. Org. Med. Chem. Lett.* 13 (2003) 1813.
- [11] M.L. Go, X. Wu, X.L. Liu, *Curr. Med. Chem.* 12 (2005) 483–499.
- [12] M.K. Pandey, S.K. Sandaur, B. Sung, G. Sethi, A.B. Kunnammakara, B.B. Aggarwal, *J. Biol. Chem.* 282 (2007) 17340–17350.
- [13] D.A. Israfi, T.A. Khaizurin, A. Syahida, N.H. Lajis, S. Khozirah, *Mol. Immunol.* 44 (2007) 673–679.
- [14] S. Kumar, A. Sharma, B. Maan, V. Singhal, B. Ghosh, *Biochem. Pharmacol.* 73 (2007) 1602–1612.
- [15] M. Funakoshi-Tago, K. Nakamura, R. Tsuruya, M. Hatanaka, T. Mashino, Y. Sonoda, T. Kasahara, *Int. Immunopharmacol.* 10 (2010) 562–571.
- [16] X. Baj, F. Cerimele, M. Ushio-Fukai, M. Waquas, P.M. Campbell, B. Govindarajan, C.J. Ber, T. Battle, D.A. Frank, K. Ye, E. Murad, W. Dubiel, G. Soff, J.L. Arbiser, *J. Biol. Chem.* 278 (2003) 35501–35507.
- [17] F. Chen, T. Wang, Y.F. Wu, Y. Gu, X.L. Xu, S. Zheng, X. Hu, *World J. Gastroenterol.* 10 (2004), 4459–3463.
- [18] L. Ma, J. Chen, X. Wang, X. Liang, Y. Luo, W. Zhu, T. Wang, M. Peng, S. Li, S. Jie, A. Peng, Y. Wei, L. Chen, *J. Med. Chem.* (2011) 6469–6481.
- [19] Y. Kuo, L. Kuo, C. Chen, *J. Org. Chem.* 62 (1997) 3242–3245.
- [20] D. Chen, S. Zhang, L. Xie, J. Xie, K. Chen, Y. Kashiwada, B. Zhou, P. Wang, L.M. Cosentino, K. Lee, *Bioorg. Med. Chem.* 5 (1997) 1715–1723.
- [21] H.G.O. Alvim, E.L. Fagg, A.L. de Oliveira, H.C.B. de Oliveira, S.M. Freitas, M.E. Xavier, T.A. Soares, A.F. Gomes, F.C. Gozzo, W.A. Silva, B.A.D. Neto, *Org. Biomol. Chem.* 11 (2013) 4764–4777.
- [22] Y. Zuo, Y. Yu, S. Wang, W. Shao, B. Zhou, L. Lin, Z. Luo, R. Huang, J. Du, X. Bu, *Eur. J. Med. Chem.* 50 (2012) 393–404.
- [23] (a) B.G. Jhonson, P.M. Gill, J.A. Pople, *J. Chem. Phys.* 98 (7) (1993) 5612–5626; (b) C. Lee, W. Yang, R.G. Parr, *Phys. Rev. B* 37 (2) (1988) 785–789.
- [24] J.M. Andrews, *J. Antimicrob. Chemother.* 48 (2001) 5–16.
- [25] G. Mengping, Z. Qiaochu, *Tetrahedron Lett.* 50 (2009) 1965–1968.
- [26] I. Fleming, *Frontier Orbitals and Organic Chemical Reactions*, Wiley, London, 1976.
- [27] C.S. Chidan kumar, C. Yohannan panicker, H. Kun Fun, Y. Sheena mary, B. Harikumar, S. Chandrāju, C.K. Quah, C.W. Ooi, *Spectrochim. Acta A.* 126 (2014) 208–219.
- [28] (a) N. Sinha, O. Prasad, V. Narayan, S.R. Shukla, *J. Mol. Simul.* 37 (2011) 153–163; (b) D.F.V. Lewis, C. Loannides, D.V. Parke, *Xenobiotica* 24 (1994) 401–408; (c) B. Kosar, C. Albayrak, *Spectrochim. Acta* 78 (2011) 160–167.
- [29] M.K. Saroj, N. Sharma, R.C. Rastogi, *J. Fluoresc.* 21 (2011) 2213–2227.
- [30] S.N. Azizi, M.J. Chaichi, M. Yousefi, *Spectrochim. Acta A Mol. Biomol. Spectrosc.* 73 (1) (2009) 101–105.
- [31] Z. Ashraf, A. Saeed, H. Nadeem, *RSC Adv.* 4 (2014) 5342.
- [32] C. Chen, J. Ke, X.E. Zhou, W. Yi, J.S. Brunzelle, J. Li, E.L. Yong, H.E. Xu, K. Melcher, *Nature* 500 (2013) 486–489.